Bivariate Statistical Modeling of Color and Range in Natural Scenes

Che-Chun Su, Lawrence K. Cormack, and Alan C. Bovik

The University of Texas at Austin, 1 University Station C1200, Austin, Texas 78712, USA

ABSTRACT

The statistical properties embedded in visual stimuli from the surrounding environment guide and affect the evolutionary processes of human vision systems. There are strong statistical relationships between co-located luminance/chrominance and disparity bandpass coefficients in natural scenes. However, these statistical relationships have only been deeply developed to create point-wise statistical models, although there exist spatial dependencies between adjacent pixels in both 2D color images and range maps.

Here we study the bivariate statistics of the joint and conditional distributions of spatially adjacent bandpass responses on both luminance/chrominance and range data of naturalistic scenes. We deploy bivariate generalized Gaussian distributions to model the underlying statistics. The analysis and modeling results show that there exist important and useful statistical properties of both joint and conditional distributions, which can be reliably described by the corresponding bivariate generalized Gaussian models. Furthermore, by utilizing these robust bivariate models, we are able to incorporate measurements of bivariate statistics between spatially adjacent luminance/chrominance and range information into various 3D image/video and computer vision applications, e.g., quality assessment, 2D-to-3D conversion, etc.

Keywords: bivariate modeling , 3D natural scene statistics

1. INTRODUCTION

Natural scene statistics (NSS) have proven to be important ingredients towards understanding both the evolution of the human vision system and the design of image processing algorithms.[1] Extensive work has been conducted towards understanding the luminance statistics of natural scenes,[2–5] and the link between natural scene statistics and neural processing of visual stimuli.[6,7] The natural scene statistics and models of 2D images have been applied to various image and video processing applications with success, e.g., image denoising[8,9] and image/video quality assessment.[10–13]

There have also been recent work conducted on modeling and understanding 3D natural scene statistics.[14–16] Potetz *et al.*[14] examined certain relationships between luminance and range over multiple scales and applied their results to shape-from-shading problems. Liu *et al.*[15] explored statistical relationships between luminance and disparity in the wavelet domain, and applied the derived models to improve a Bayesian stereo algorithm. Recently, Su *et al.*[16] proposed robust and reliable statistical models of both marginal and conditional distributions of luminance/chrominance and disparity in natural images, and further incorporate these models into a chromatic Bayesian stereo algorithm with superior performance to luminance-only algorithms.

However, little work has been done on modeling and using the bivariate statistics of luminance/chrominance and range data from naturalistic scenes. Here we aim to fill this gap using the high-definition, high-quality color images and corresponding ground-truth range maps from the LIVE Color+3D Database Release-1.[17] We first studied the joint statistics of spatially adjacent wavelet coefficients at each sub-band for both luminance/chrominance and range, and also examined the bivariate conditional distributions of luminance and chrominance wavelet coefficients given different values of co-located range wavelet coefficients. To model these bivariate statistics, we utilized the relevant, versatile and flexible multivariate generalized Gaussian distributions

Further author information: (Send correspondence to Che-Chun Su)
Che-Chun Su: E-mail: ccsu@utexas.edu

Human Vision and Electronic Imaging XIX, edited by Bernice E. Rogowitz, Thrasyvoulos N. Pappas, Huib de Ridder, Proc. of SPIE-IS&T Electronic Imaging, Proc. of SPIE Vol. 9014, 90141G
 · doi: 10.1117/12.2036505

(MGGD). We discovered some interesting and important statistical properties of both bivariate joint and conditional distributions, and showed that they are well-modeled by appropriate choice of the fitting parameters of bivariate generalized Gaussian models.

The rest of this paper is organized as follows. Section 2 details the types of perceptually relevant pre-processing that is performed on both the 2D color images and ground-truth range maps. The statistical analysis and modeling are presented in Section 3. Finally, Section 4 gives concluding remarks.

2. DATA PRE-PROCESSING

The basic resource on which we perform bivariate statistical modeling on natural image and range data is the LIVE Color+3D Database Release-1, which contains 12 sets of color images with corresponding ground-truth range maps at a high-definition resolution of 1280x720.[17] The image and range data in the LIVE Color+3D Database Phase-1 were collected using an advanced range scanner, RIEGL VZ-400, with a Nikon D700 digital camera mounted on top of it.[18]

Human vision systems extract abundant information from natural environments by processing visual stimuli through different levels of decomposition and interpretation. Since we want to learn and explore the statistical relationships between luminance/chrominance and range information carried in natural images, and how these statistics might be implicated in visual processing, we apply certain perceptually relevant pre-processing steps on both the 2D color images and the co-registered 2D ground-truth range maps.

2.1 Luminance/Chrominance

All color images were first transformed into the perceptually relevant CIELAB color space with one luminance (L*) and two chrominance (a* and b*) components. CIELAB color space is optimized to quantify perceptual color differences and better corresponds to human color perception than does the perceptually nonuniform RGB space.[19] Each image was then transformed by the steerable pyramid decomposition, which is an over-complete wavelet transform that allows for increased orientation selectivity.[20] Use of the wavelet transform was motivated by the fact that its space-scale-orientation decomposition resembles the bandpass filtering that occurs in area V1 of the primary visual cortex.[2,21]

After applying the multi-scale, multi-orientation decomposition, we performed the perceptually significant process of divisive normalization on the image wavelet coefficients at all sub-bands.[22] Divisive normalization, i.e., sensory gain control, was proposed in the psychophysical literature to account for the nonlinear behavior of human perceptual neurons.[23] In human vision systems, divisive normalization corresponds to contrast gain control, where the response of a neuron is normalized based on the responses of a pool of its neighboring neurons, and partially explains the contrast masking mechanism. Moreover, divisive normalization also reduces statistical dependencies between neural responses within and/or across different sub-bands.

The divisive normalization transform (DNT) used in this paper is implemented as follows:[24]

$$u_i = \frac{x_i}{\sqrt{\alpha + \mathbf{x_g}^T \mathbf{x_g}}} = \frac{x_i}{\sqrt{\alpha + \sum_j g_j x_j^2}} \tag{1}$$

where i is the current pixel location, x_i represents the wavelet coefficients, u_i represents the coefficients after DNT, α is a semi-saturation constant, the sum occurs over neighborhood pixels indexed by j, and $\{g_j\}$ is a Gaussian weighting function.

2.2 Range

Since the depth information acquired by human vision systems is more relative than absolute, the disparity, i.e., the reciprocal of range, serves as a more useful stereoscopic analytic cue and disparity statistics are a useful tool for understanding depth perception. In the absence of measured visual fixations, we took the reciprocal values of all ground-truth range maps, and then performed the same multi-scale, multi-orientation wavelet decomposition and divisive normalization transform on them. In the next section, we detail results of statistical modeling of both the joint and conditional bivariate distributions of the image and range wavelet coefficients following DNT.

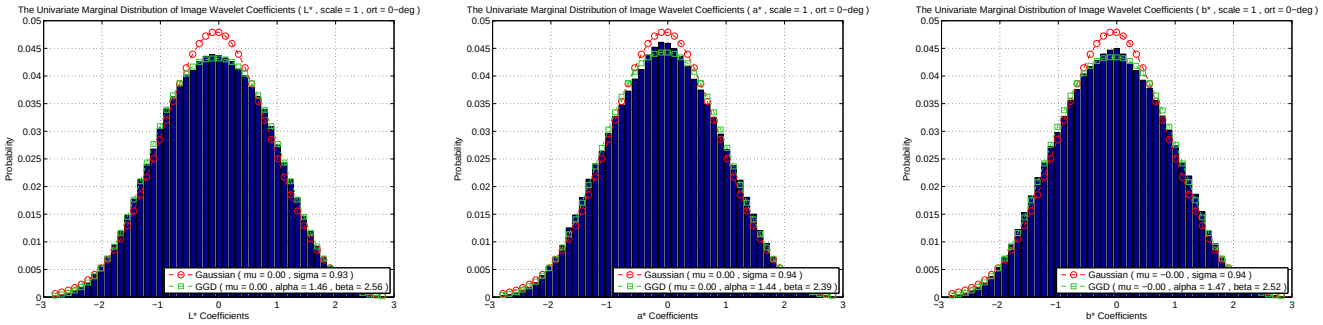

(a) L* (b) a* (c) b*

Figure 1. Marginal univariate distributions of image wavelet coefficients at scale = 1 and orientation = 0°.

3. BIVARIATE STATISTICAL MODELING

It has been demonstrated that there exist strong statistical relationships between co-located luminance/chrominance and disparity bandpass coefficients, where the corresponding magnitudes can be well modeled by univariate generalized log-normal distributions.[16] However, there still exist higher-order dependencies between neighboring pixels in natural images and range maps, where reliable statistical models remain. In the following, we study the statistical relationships between spatially adjacent pixels in natural images and range maps, and model both their joint and conditional bivariate distributions.

3.1 Multivariate Generalized Gaussian Distribution

It is well known that the histograms of sub-band coefficients of natural images become more Gaussian-like after divisive normalization, as compared to their Laplacian-like nature before normalization. However, we found that after performing DNT, the joint statistics of spatially adjacent sub-band coefficients of natural images possess interesting orientation-related dependencies, which no longer can be modeled as bivariate Gaussian distributions. In order to model both the univariate and bivariate statistics of sub-band coefficients of natural images, we utilized the multivariate generalized Gaussian distribution, which includes the multivariate Gaussian and multivariate Laplace distributions as special cases.

The probability density function of a multivariate generalized Gaussian distribution (MGGD) is defined as:

$$p(\mathbf{x}|\mathbf{M},\alpha,\beta) = \frac{1}{|\mathbf{M}|^{\frac{1}{2}}} g_{\alpha,\beta}(\mathbf{x}^T\mathbf{M}^{-1}\mathbf{x}) \tag{2}$$

where $\mathbf{x} \in \mathbb{R}^N$, $\mathbf{M}$ is an $N \times N$ symmetric scatter matrix, α and β are the scale and shape parameters, respectively, and $g_{\alpha,\beta}(\cdot)$ is the density generator:

$$g_{\alpha,\beta}(y) = \frac{\beta\Gamma(\frac{N}{2})}{(2^{\frac{1}{\beta}}\pi\alpha)^{\frac{N}{2}}\Gamma(\frac{N}{2\beta})} e^{-\frac{1}{2}(\frac{y}{\alpha})^{\beta}} \tag{3}$$

where $y \in \mathbb{R}^+$. Note that when $\beta = 0.5$, Eq. (2) becomes the multivariate Laplacian distribution, and when $\beta = 1$, Eq. (2) corresponds to the multivariate Gaussian distribution. Moreover, when $\beta \to \infty$, the MGGD converges to a multivariate uniform distribution.

To fit an MGGD model to the bivariate histogram of spatially adjacent sub-band coefficients of a natural image and to find the corresponding model parameters, we adopt the maximum likelihood estimator (MLE) algorithm.[25] Specifically, when the shape parameter, β, of the MGGD model is unknown, the MLEs of parameters $\mathbf{M}$, α, and β can be obtained by differentiating the log-likelihood of $p(\{\mathbf{x}_1,\cdots,\mathbf{x}_K\}|\mathbf{M},\alpha,\beta)$, where $\{\mathbf{x}_1,\cdots,\mathbf{x}_K\}$ are K independent and identically distributed (i.i.d.) MGGD random vectors, with respect to $\mathbf{M}$, α, and β. This

yields the MLEs of the parameters $\mathbf{M}$, α, and β, as below.

$$\mathbf{M} = \frac{1}{K}\sum_{k=1}^{K}\left[\frac{NK}{y_k + y_k^{1-\beta}\sum_{j\neq k}^{K} y_j^{\beta}}\mathbf{x}_k\mathbf{x}_k^T\right] \tag{4}$$

$$\alpha = \left[\frac{\beta}{NK}\sum_{k=1}^{K} y_k^{\beta}\right]^{\frac{1}{\beta}} \tag{5}$$

$$f(\beta) = \frac{NK}{2\sum_{k=1}^{K} y_k^{\beta}}\sum_{k=1}^{K}\left[y_k^{\beta}\ln(y_k)\right] - \frac{NK}{2\beta}\left[\Psi\left(\frac{N}{2\beta}\right) + \ln\left(\frac{2\beta}{NK}\sum_{k=1}^{K} y_k^{\beta}\right)\right] - K = 0 \tag{6}$$

where $y_k = \mathbf{x}_k^T\mathbf{M}^{-1}\mathbf{x}_k$ and $\Psi(\cdot)$ is the digamma function, which is the logarithmic derivative of the gamma function, i.e., $\Psi(x) = \frac{d}{dx}\ln(\Gamma(x))$.

Note that the MLEs of $\mathbf{M}$ and β depend on each other, while α can be estimated directly from β. The following iterative algorithm yields MLEs of the MGGD model parameters.

Algorithm 1 Estimate the MGGD parameters using the MLEs

```
Initialize M and β
for i = 1 to max_num_iter do
    Estimate M using Eq. (4).
    Estimate β using Eq. (6) via the Newton-Raphson method:
```

$$\beta_i = \beta_{i-1} - \frac{f(\beta_{i-1})}{f'(\beta_{i-1})} \tag{7}$$

```
    if |β_i − β_{i−1}| ≤ fitting_error then
        break
    end if
end for
Estimate α using Eq. (5).
```

Figure 1 histograms both the luminance and chrominance wavelet coefficients of one sub-band following DNT, along with their univariate Gaussian and generalized Gaussian fits. We can see that although the image sub-band coefficients after DNT are reasonably well fitted by the univariate Gaussian distribution, the univariate GGD is able to give an even better fit.

3.2 Joint Distribution and Bivariate GGD Fit

First of all, we examine the joint distribution of spatially adjacent wavelet coefficients following DNT on both color images and ground-truth range maps at different sub-bands. We utilize the steerable pyramid decomposition with five scales, from 1 (finest) to 5 (coarsest), and eight orientations, i.e., 0°, 22.5°, ..., 157.5°. Note that the orientation is defined as the propagation direction of the sinusoidal signal used in the bandpass filtering.

We focus on two cases of spatial adjacency between bandpass responses: horizontal and vertical adjacency. Specifically, for horizontally adjacent bandpass samples, we form an N-by-2 matrix, where N is the total number of pairs of samples from the database, where each pair is sampled from locations (x, y) and $(x + 1, y)$ of an image or range map. Similarly, for vertically adjacent samples, each pair is sampled from the locations (x, y) and $(x, y + 1)$. We observed that similar statistics hold with consequent similar models for both horizontal and vertical adjacency; hence, we will discuss the results only for the horizontal case hereafter, unless otherwise explicitly stated.

The joint histograms of both luminance/chrominance and range wavelet coefficients after DNT were computed from all the N row vectors $\in \mathbb{R}^2$ in the corresponding N-by-2 matrix. Thus, the bivariate generalized Gaussian models are fitted by estimating the parameters $\mathbf{M}$, α, and β using algorithm 1 with $N = 2$.

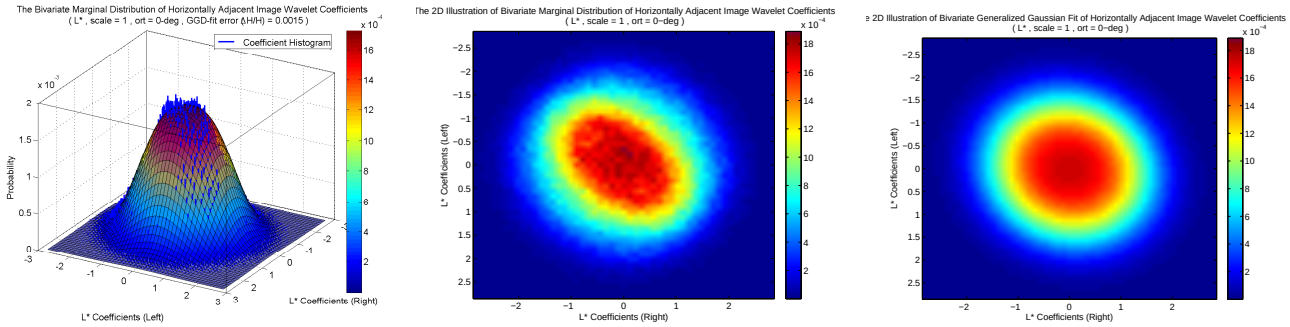

(a) Bivariate GGD fit (b) 2D illustration of histogram (c) 2D illustration of bivariate GGD fit

Figure 2. Joint distribution and bivariate GGD fit of image L* wavelet coefficients at scale = 1 and orientation = 0°.

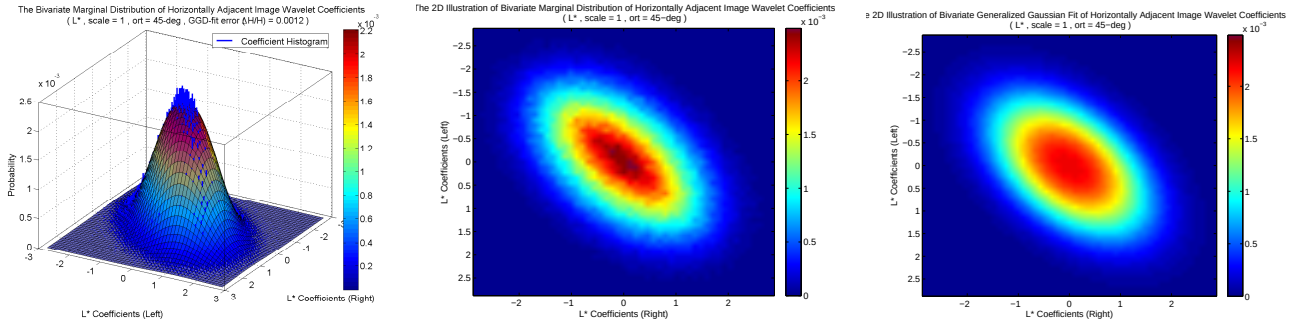

(a) Bivariate GGD fit (b) 2D illustration of histogram (c) 2D illustration of bivariate GGD fit

Figure 3. Joint distribution and bivariate GGD fit of image L* wavelet coefficients at scale = 1 and orientation = 45°.

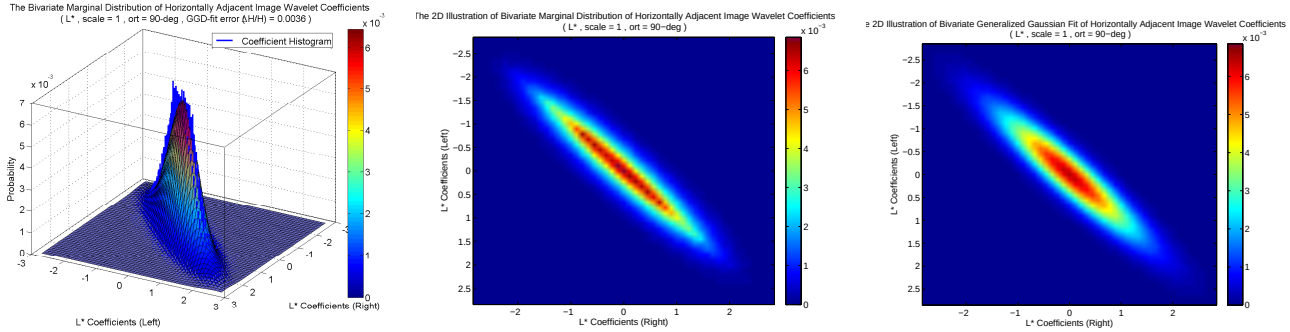

(a) Bivariate GGD fit (b) 2D illustration of histogram (c) 2D illustration of bivariate GGD fit

Figure 4. Joint distribution and bivariate GGD fit of image L* wavelet coefficients at scale = 1 and orientation = 90°.

Figure 2 to 4 show the joint empirical distributions and the corresponding bivariate GGD (BGGD) fits of luminance L* wavelet coefficients at scale = 1 and three different orientations. From the three-dimensional illustrations, where the blue bars represent the actual coefficient histograms and the colored meshes represent the bivariate GGD fits, it can be seen that the joint distributions of L* wavelet coefficients are well modeled as bivariate generalized Gaussian. The 2D illustrations, which show the iso-probability contour maps of the joint distributions, also illustrate the close fit of the bivariate GGD model. The most important observation is that the shape and height of the joint distributions both vary with the relative orientation of the sub-band. In particular, when the spatial relationship between bandpass samples, e.g., horizontal, matches the sub-band orientation, e.g., 90°, then the joint distribution becomes peaky and extremely elliptical. On the other hand, when the spatial relationship and the sub-band orientation are orthogonal, e.g., horizontal and 0°, then the joint distribution becomes nearly a circular Gaussian. This implies that there exist higher dependencies between spatially adjacent L* bandpass samples that have relative orientation that matches the sub-band orientation. Note that similar results are obtained on both chrominance and range wavelet coefficients, which are not shown here due to space limits.

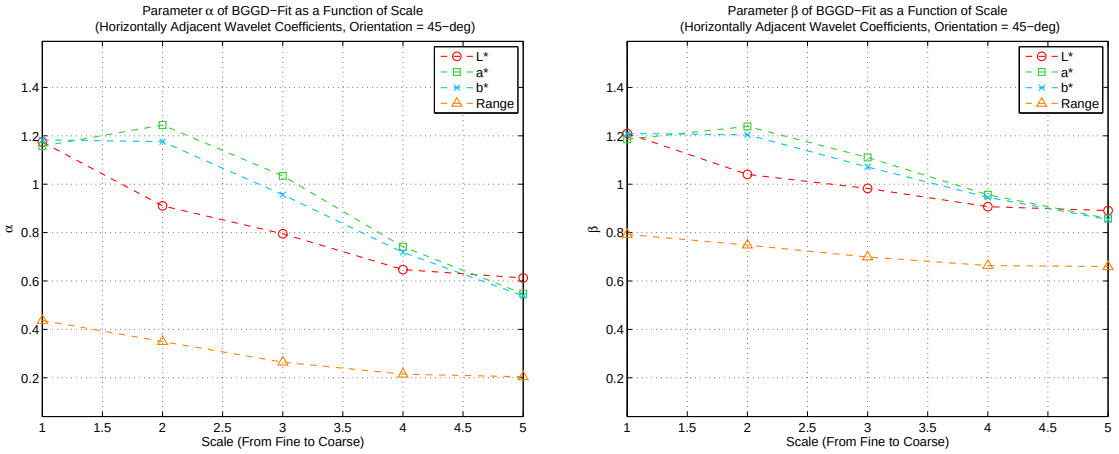

(a) α (b) β

Figure 5. Parameters of joint bivariate GGD fit as a function of scale at orientation = 45°.

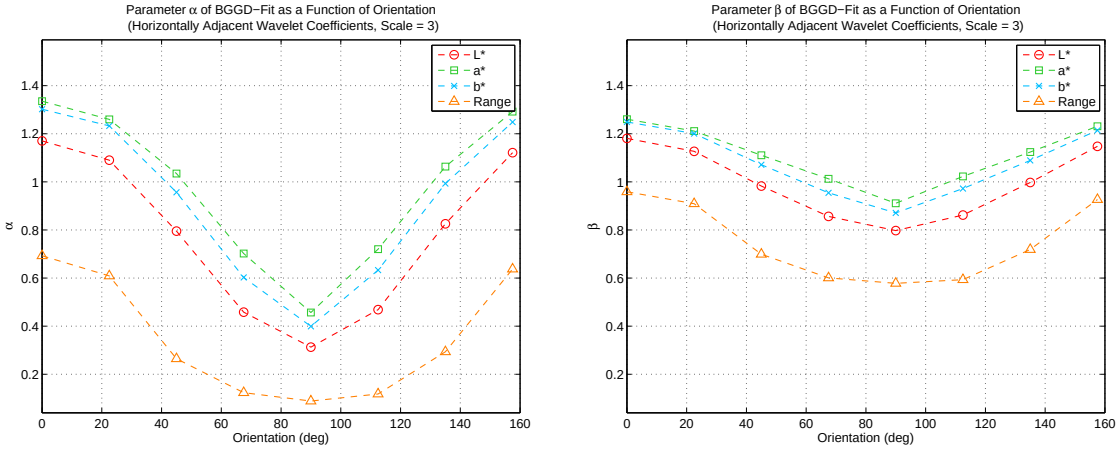

(a) α (b) β

Figure 6. Parameters of joint bivariate GGD fit as a function of orientation at scale = 3.

To further examine the sub-band dependency of luminance, chrominance, and range wavelet coefficients, we plot the bivariate GGD model parameters, i.e., α and β, both as a function of scale at the same orientation, and as a function of orientation at the same scale. Figure 5 plots the bivariate GGD fitting parameters as a function of scale at orientation = 45°, while Figure 6 plots the parameters as a function of orientation at scale = 3. As the scale becomes coarser, both parameters α and β decrease monotonically, meaning that the corresponding bivariate GGD fit becomes more peaky and elliptical. In other words, spatially adjacent wavelet coefficients tend to possess higher dependencies at larger scales on both luminance/chrominance and range in natural scenes. Figure 6 shows the strong orientation dependency of both parameters α and β, which reach a minimum when the spatial relationship of adjacent pixels matches the sub-band orientation, meaning that the corresponding spatially adjacent coefficients possess the highest dependencies compared to other sub-bands orientations. These scale- and orientation-dependent statistics also match what can be observed from both the 3D and 2D illustrations as shown in Figure 2 to 4.

In fact, we can examine these statistical dependencies from another, probably more intuitive, perspective in terms of correlation coefficients. Figure 7 shows the plots of correlation coefficients between horizontally adjacent luminance/chrominance and range wavelet coefficients as a function of scale and orientation. It is apparent from Figure 7(a), with the same sub-band orientation, e.g., 90°, that the two horizontally adjacent wavelet coefficients are highly correlated, with correlation coefficients larger than 0.9. As the scale becomes coarser, the correlation coefficients also become even larger. On the other hand, Figure 7(b) clearly indicates that at the same sub-band

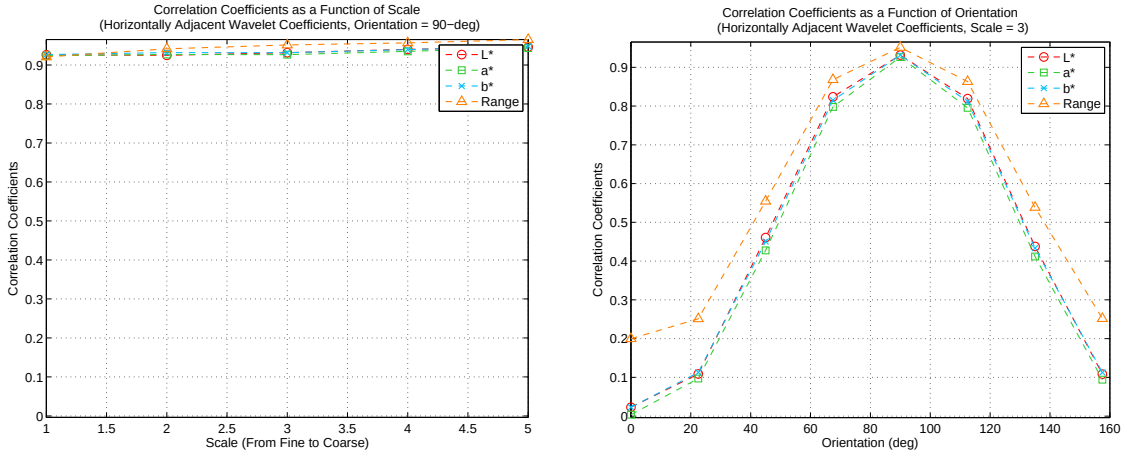

(a) As a function of scale at orientation = 90° (b) As a function of orientation at scale = 3

Figure 7. Correlation coefficients of horizontally adjacent wavelet coefficients as a function of scale and orientation.

scale, the horizontally adjacent wavelet coefficients are most correlated when the orientation of bandpass filtering aligns at 90°. These statistics relating the correlation coefficients between spatially adjacent wavelet coefficients again substantiate the scale and orientation dependencies found in Figure 2 to 6.

3.3 Conditional Distribution and Bivariate GGD Fit

In addition to the rich information embedded in the joint statistical models of luminance/chrominance and range wavelet coefficients, we are also interested in exploring the conditional statistics and models between luminance/chrominance and range data in natural scenes. Interesting past work has been directed towards utilizing conditional statistical models between luminance/chrominance and range wavelet coefficients to improve the performance of practical stereo algorithms.[15,16] However, to our knowledge, there hasn't been reported work on bivariate modeling of any form of conditional distributions between luminance/chrominance and range data in natural scenes. Therefore, we also examined the bivariate distributions of spatially adjacent luminance and chrominance wavelet coefficients conditioned on co-located range wavelet coefficients.

Specifically, we first sampled and collected the range wavelet coefficients after DNT from all ground-truth maps in the database. Then, we also collected the co-located pairs of spatially adjacent luminance/chrominance wavelet coefficients. For example, if the range wavelet coefficient at (x, y) was collected, then the pair of image wavelet coefficients at (x, y) and $(x + 1, y)$ (for horizontally adjacent pixels), or at (x, y) and $(x, y + 1)$ (for vertically adjacent pixels), were also collected. Next, we created a number of bins based on the absolute value of the range wavelet coefficients, and for each range bin, we collected the corresponding pairs of spatially adjacent luminance/chrominance wavelet coefficients. Finally, the conditional bivariate distribution of spatially adjacent image wavelet coefficients given range wavelet coefficients is built as the bivariate joint distribution of spatially adjacent luminance/chrominance wavelet coefficients, as described in Section 3.2, within each bin of the range wavelet coefficients.

Figure 8 shows the conditional distributions of horizontally adjacent L* wavelet coefficients given different bins of range wavelet coefficients at one sub-band, scale = 3 and orientation = 90°, and their corresponding bivariate GGD fits. As observed in the case of bivariate joint distributions of spatially adjacent wavelet coefficients in Section 3.2, the bivariate conditional distributions also possess peaky and elliptical natures when the spatial relationship between wavelet coefficients align with the sub-band orientation. An important observation here is that the shape and height of the bivariate conditional distribution remains almost the same across different range bins. Moreover, in Figure 9 we plot the parameters, α and β, of the bivariate GGD fits as a function of range bin at the same sub-band as in Figure 8. We can clearly see that both fitting parameters remain constant as the range bin varies, supporting the observations from Figure 8.

Similar to the analysis of the bivariate joint distribution in Section 3.2, we also computed and examined the correlation coefficients between spatially adjacent luminance/chrominance wavelet coefficients conditioned on

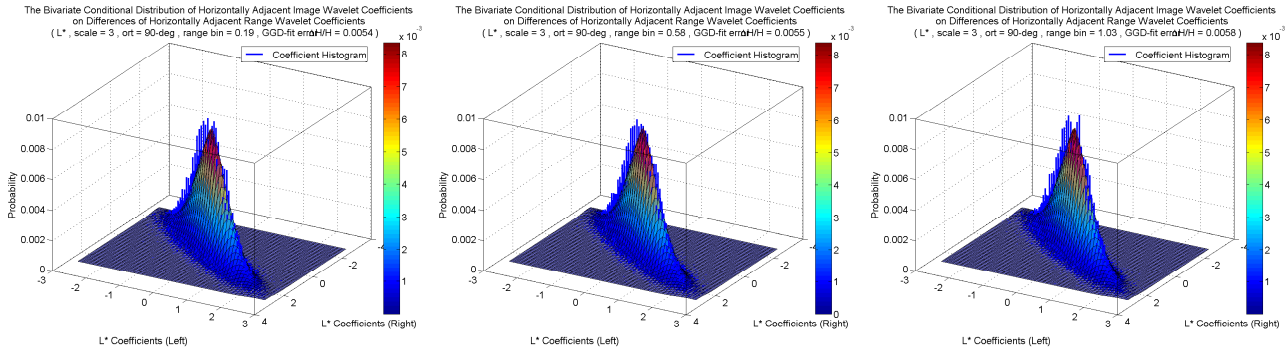

(a) Range bin #2 (b) Range bin #5 (c) Range bin #8

Figure 8. Conditional distribution and bivariate GGD fit of image L* wavelet coefficients on different range bins at scale = 3 and orientation = 90°.

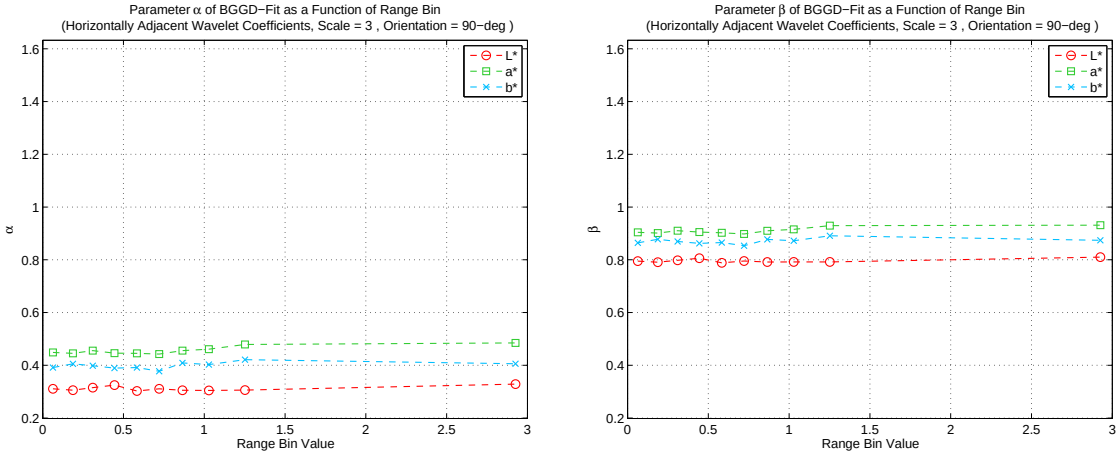

(a) α (b) β

Figure 9. Parameters of conditional bivariate GGD fit as a function of range bin at scale = 3 and orientation = 90°.

different bins of range wavelet coefficients. Figure 10 shows the plots of correlation coefficients between spatially adjacent luminance/chrominance wavelet coefficients as a function of range bin for four different orientations, 0°, 45°, 90°, and 135°, at the same scale = 3. In addition to the same orientation dependency, where the correlation coefficient of spatially adjacent image wavelet coefficients reaches a maximum when the spatial relationship between wavelet coefficients aligns with the sub-band orientation and a minimum when orthogonal, the correlation coefficients remain the same across different range bins, reinforcing the invariance property of the conditional statistics observed in Figure 8 and 9.

4. CONCLUSIONS

We have studied both the joint and conditional distributions of spatially adjacent luminance/chrominance and range wavelet coefficients in natural scenes, and modeled them using the relevant, versatile and flexible bivariate generalized Gaussian distributions. We discover several interesting as well as important statistical properties from these bivariate GGD models.

Specifically, there are both scale and orientation dependencies embedded in the joint distributions of spatially adjacent luminance/chrominance and range wavelet coefficients. Spatially adjacent pairs of wavelet coefficients in both natural images and ground-truth maps are highly correlated when decomposed by a bandpass filter whose orientation is parallel to their spatial relationship; however, these pairs of wavelet coefficients become almost uncorrelated when their spatial relationship and the sub-band orientation are orthogonal. Moreover, when conditioned on different values of range wavelet coefficients, both luminance and chrominance coefficients maintain constant correlation coefficients between spatially adjacent wavelet coefficients. These joint scale and orientation

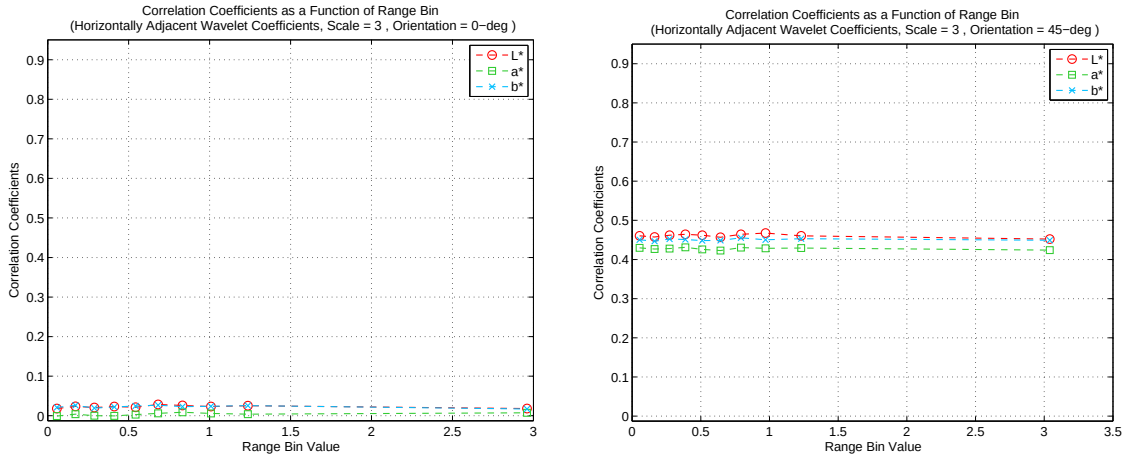

(a) At orientation = 0°

(b) At orientation = 45°

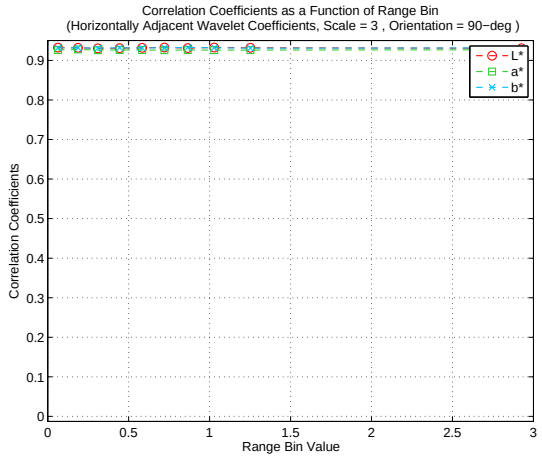

(c) At orientation = 90°

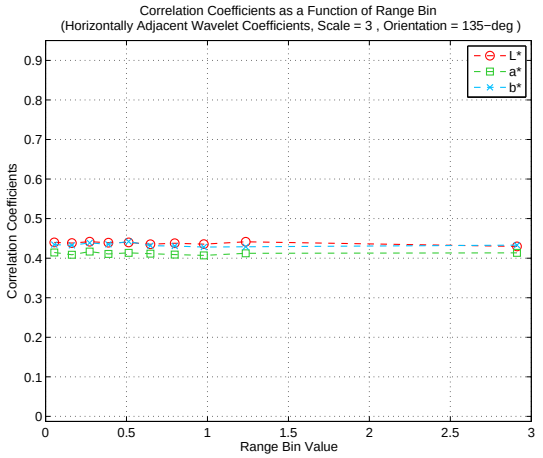

(d) At orientation = 135°

Figure 10. Correlation coefficients of spatially neighboring wavelet coefficients as a function of range bin for four different orientations at the same scale = 3.

dependencies, as well as the conditional invariant correlation are effectively captured by the parameters of the corresponding bivariate GGD models.

We believe that these bivariate statistics and models will help us better understand the processing of three-dimensional visual stimuli in human vision systems, and will also benefit perception-driven 3D image/video and computer vision applications, e.g., 3D quality assessment, 2D-to-3D conversion, etc.

ACKNOWLEDGMENTS

This research was supported by the National Science Foundation under grants IIS-0917175 and IIS-1116656.

REFERENCES

[1] Wang, Z. and Bovik, A. C., "Reduced- and no-reference image quality assessment: The natural scene statistic model approach," *IEEE Signal Processing Magazine* **28**, 29–40 (Nov. 2011).

[2] Field, D. J., "Relations between the statistics of natural images and the response properties of cortical cells," *Journal of the Optical Society of America A* **4**(12), 2379–2394 (1987).

[3] Ruderman, D. L. and Bialek, W., "Statistics of natural images: Scaling in the woods," *Physical Review Letters* **73**, 814–817 (Aug. 1994).

[4] Field, D. J., "Wavelets, vision and the statistics of natural scenes," *Philosophical Transactions of the Royal Society of London. Series A: Mathematical, Physical and Engineering Sciences* **357**(1760), 2527 (1999).
[5] Srivastava, A., Lee, A. B., Simoncelli, E. P., and Zhu, S.-C., "On advances in statistical modeling of natural images," *Journal of Mathematical Imaging and Vision* **18**(1), 17–33 (2003).
[6] Simoncelli, E. P. and Olshausen, B. A., "Natural image statistics and neural representation," *Annual Review of Neuroscience* **24**, 1193–1216 (Mar. 2001).
[7] Geisler, W. S., "Visual perception and the statistical properties of natural scenes," *Annual Review of Psychology* **59**, 167–192 (Jan. 2008).
[8] Portilla, J., Strela, V., Wainwright, M. J., and Simoncelli, E. P., "Image denoising using scale mixtures of gaussians in the wavelet domain," *IEEE Transactions on Image Processing* **12**, 1338–1351 (Nov. 2003).
[9] Cho, D. and Bui, T. D., "Multivariate statistical modeling for image denoising using wavelet transforms," *Signal Processing: Image Communication* **20**, 77–89 (Jan. 2005).
[10] Sheikh, H. and Bovik, A., "Image information and visual quality," *IEEE Transactions on Image Processing* **15**, 430–444 (Feb. 2006).
[11] Seshadrinathan, K. and Bovik, A. C., "Motion tuned spatio-temporal quality assessment of natural videos," *IEEE Transactions on Image Processing* **19**, 335–350 (Feb. 2010).
[12] Soundararajan, R. and Bovik, A., "RRED indices: Reduced reference entropic differencing for image quality assessment," *IEEE Transactions on Image Processing* **21**, 517–526 (Feb. 2012).
[13] Moorthy, A. K. and Bovik, A. C., "Blind image quality assessment: From natural scene statistics to perceptual quality," *IEEE Transactions on Image Processing* **20**, 3350–3364 (Dec. 2011).
[14] Potetz, B. and Lee, T. S., "Scaling laws in natural scenes and the inference of 3D shape," *Advances in Neural Information Processing Systems* **18**, 1089–1096 (2006).
[15] Liu, Y., Cormack, L. K., and Bovik, A. C., "Statistical modeling of 3-D natural scenes with application to bayesian stereopsis," *IEEE Transactions on Image Processing* **20**, 2515–2530 (Sep. 2011).
[16] Su, C.-C., Cormack, L. K., and Bovik, A. C., "Color and depth priors in natural images," *IEEE Transactions on Image Processing* **22**, 2259 – 2274 (June 2013).
[17] Su, C.-C., Cormack, L. K., and Bovik, A. C., "LIVE Color+3D Database - Release 1." `http://live.ece.utexas.edu/research/3dnss/live_color_plus_3d.html`.
[18] RIEGL, "RIEGL VZ-400 3D Terrestrial Laser Scanner." `http://rieglusa.com/products/terrestrial/vz-400/index.shtml`.
[19] Rajashekar, U., Wang, Z., and Simoncelli, E. P., "Perceptual quality assessment of color images using adaptive signal representation," *SPIE Int. Conf. on Human Vision and Electronic Imaging* **7527** (Jan. 2010).
[20] Simoncelli, E. P. and Freeman, W. T., "The steerable pyramid: A flexible architecture for multi-scale derivative computation," *IEEE International Conference on Image Processing* **3**, 444–447 (Oct. 1995).
[21] Olshausen, B. A. and Field, D. J., "How close are we to understanding V1?," *Neural Computation* **17**, 1665–1699 (Aug. 2005).
[22] Wainwright, M. J., Schwartz, O., and Simoncelli, E. P., "Natural image statistics and divisive normalization: Modeling nonlinearity and adaptation in cortical neurons," *Probabilistic Models of the Brain: Perception and Neural Function* , 203–222 (Feb. 2002).
[23] Schwartz, O. and Simoncelli, E. P., "Natural signal statistics and sensory gain control," *Nature Neuroscience* **4**, 819–825 (Aug. 2001).
[24] Lyu, S., "Dependency reduction with divisive normalization: justification and effectiveness," *Neural Computation* **23**, 2942–2973 (2011).
[25] Bombrun, L., Pascal, F., Tourneret, J.-Y., and Berthoumieu, Y., "Performance of the maximum likelihood estimators for the parameters of multivariate generalized gaussian distributions," *IEEE International Conference on Acoustic, Speech and Signal Processing* , 3525–3528 (2012).